

MOLYBDENUM DICHALCOGENIDE CATHODES FOR ALUMINIUM-ION BATTERIES

A PREPRINT

Shalini Divya, James H. Johnston
School of Chemical and Physical Sciences
Victoria University of Wellington
Wellington, New Zealand

Thomas Nann*
School of Mathematical and Physical Sciences
The University of Newcastle
Callaghan, NSW 2308, Australia
thomas.nann@newcastle.edu.au

September 2, 2022

ABSTRACT

Many successful battery electrodes are based on 2D-layered materials. We have studied aluminium-ion batteries using molybdenum dichalcogenides: MoS_2 , MoSe_2 and MoSSe as active cathode materials. The batteries showed clear discharge voltage plateaus in the ranges 1.6 - 1.4 V for MoS_2 and MoSe_2 , and 0.6 - 0.5 V for MoSSe . MoS_2 and MoSe_2 have similar crystal structures, interestingly we found that MoSe_2 performed better than MoS_2 . MoSSe exhibited a higher specific capacity over MoS_2 and MoSe_2 , but the energy density was lower than MoSe_2 at a current rate of 40 mA g^{-1} . MoSe_2 cells recorded a discharge capacity of $\sim 110 \text{ mAh g}^{-1}$ with an average potential at $\sim 2.0 \text{ V}$. The cells were stable at 100 mA g^{-1} for over 200 cycles with 90% coulombic efficiency.

Keywords Aluminium-ion battery · Layered compounds · Molybdenum dichalcogenides · Cathode · Electrochemistry

1 Introduction

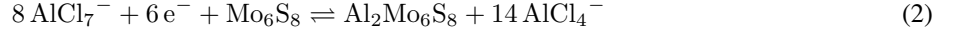
Aluminium-ion batteries (AIBs) offer an alternative to the prevalent lithium-ion battery (LIB) technology. Aluminium being the most abundant metal in the Earth's crust, these batteries will not only be much cheaper, but hold promise to solve other problems such as recyclability and thermal runaway. Furthermore, the multivalent nature of aluminium may result in a higher specific capacity and energy density compared with other monovalent battery types. Research on AIBs is still in its early stages and current work focuses mainly on electrolytes and cathode materials. In this article, we explore different molybdenum dichalcogenide-based materials and their mechanism of energy storage. We expected that two-dimensional (2D) layered materials that support intercalation of charged species might be suitable as active cathode materials in AIBs.

The most common AIB electrolyte is currently the ionic liquid 1-ethyl-3-methylimidazolium/tetrachloroaluminate ($[\text{EMIm}]^+/\text{AlCl}_4^-$), although many other alternatives are under investigation [1]. The most studied cathode types are graphite-based, where chloroaluminate ions AlCl_4^- have been shown to intercalate/deintercalate during the charging/discharging processes. Various forms of graphite such as fluorinated graphite [2], Kish graphite flakes [3], three-dimensional graphitic foam [4], few-layer graphene aerogels [5], and several others have been tested. Analytical techniques such as X-ray diffraction (XRD), Raman spectroscopy and X-ray photoelectron spectroscopy (XPS) have been used broadly to verify the intercalation/deintercalation mechanism.

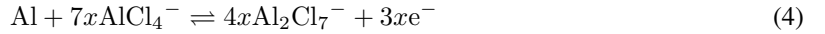
Molybdenum dichalcogenides (MoX_2 where $\text{X}=\text{S}, \text{Se}$ or Te) display similar properties as graphite. They have a 2D-layered structure, which allows intercalation of ions and are electrically conductive. Lower volumetric expansion on cycling is an advantage these materials have over graphitic cathodes [6, 7]. Amongst various transition metal chalcogenides, MoS_2 has been extensively studied as a cathode for rechargeable batteries [8, 9], making them attractive candidates for AIB cathodes. In 2015, Geng *et al.* found that Al^{3+} ions fully intercalated into chevrel phase Mo_6S_8

*Corresponding author.

with the cations occupying two different sites in the crystal lattice [10]. This mechanism was called the 'rocking chair' mechanism where charge carrying species shuttled back and forth between intercalating electrodes during cycles while the overall electrolyte concentration remains constant. The discharging and charging reactions at the anode (equation 1) and cathode (equation 2) were proposed as follows:



Three years later, Li *et al.* prepared MoS_2 microspheres by a simple hydrothermal method [11]. They proposed a similar mechanism where Al^{3+} ions inserted into the electrode accompanied by a phase transformation at the electrode interface. Li and his group confirmed this phase-transition by using *ex-situ* XPS and XRD etching techniques. The reaction equations for this battery system at the cathode (equation 3) and anode (equation 4) were proposed as follows:



In general, these cells showed low energy density and had reversibility issues in the redox processes. It has been reported that transition metal dichalcogenide electrodes tend to transition from a 2H phase into a more conducting 1T phase when used in a battery [12]. A hybrid $\text{Mg}^{2+}/\text{Li}^+$ cell was tested using bulk MoS_2 as a cathode material. During cyclic voltammetry (CV) scans, the authors associated the first cathodic peak, with a phase transition. 2H phase MoS_2 was converted to 1T phase during initial ion intercalation. This seems to be a common phenomenon for molybdenum dichalcogenides, since Li *et al.* observed similar transitions in sodium ion batteries [13]. It mostly takes place during the first cycle and since the phase change is irreversible, it can be detected in a cyclic voltammogram.

In this work, we studied a range of 2D molybdenum dichalcogenides including MoS_2 , MoSe_2 and MoSSe , and tested them as cathodes for non-aqueous AIBs. Our unpublished, preliminary density functional theory (DFT) calculations indicated a significant decrease in inter-layer spacing of these materials when Al^{3+} cations were assumed to intercalate (owing to the very high charge density of Al^{3+}). Therefore, we propose intercalation of structurally distorted AlCl_4^- anions into the cathode layers. Surprisingly we found that MoSe_2 -based cathodes performed different and better than all of the other molybdenum dichalcogenides.

2 Results and Discussion

Figure 1 shows the crystal structure of MoX_2 where X is sulfur (S) and/or selenium (Se). The material has two vacant sites for intercalation — M1 and M2. M1 denotes the spaces in between the X-Mo-X atoms, whereas M2 represents the space created between the MoX_2 layers as shown in Figure 1 a). The inter-layer distance in MoX_2 is 6.3 Å with a gallery height of 3 Å. The layers are held together by weak van der Waals (vdW) forces. M2 presents an open network and provides various interstitial sites for intercalation. Since AlCl_4^- ions are 5.28 Å in diameter, as reported by Takahashi *et al.* [14], they undergo some distortion during intercalation to fit into these layers. Our preliminary results showed that Al^{3+} would 'contract' the MoX_2 layers when trying to intercalate, making AlCl_4^- anion intercalation more likely. Also, the triply charged Al^{3+} cation has to overcome strong electrostatic forces from the S^{2-} or Se^{2-} anion network in order to enter, making the intercalation process slow and most likely not reversible. Therefore, we propose intercalation of AlCl_4^- anions from the electrolyte into M2 sites of MoX_2 during charge. Galvanostatic cycles, cyclic voltammetry (CV), X-Ray diffraction (XRD), Raman spectra and X-Ray Photoelectron Spectroscopy (XPS) results discussed later, strongly support our claim of a reversible intercalation process especially in MoSe_2 .

A modified two-electrode polyether ether ketone (PEEK) cell (Figure 2) was used for conducting preliminary electrochemical tests. Electrode preparation and cell configuration are described in the Experimental Methods section.

Figure 3 a)–c) shows the charge/discharge cycles (CDCs) for MoS_2 , MoSe_2 and MoSSe at a current rate of 40 mA g^{-1} . The discharge capacity of Al/MoS_2 in its first cycle was found at $\sim 45 \text{ mAh g}^{-1}$, Figure 3 a). Comparing this with its first CV scan (Figure 3 g), a good correlation between the discharge voltage plateau and reduction peaks, and other redox features was found. With discharge plateaus at 1.9 V and 1.7 V, the first CV scan for MoSe_2 displayed two reduction peaks at 1.65 V (point A) and 1.0 V (point B), Figures 3 b) and 3 h). The peak at 1.0 V suggested an irreversible reaction since this peak was absent in the following scans. Based on this, we agree with Li *et al.*'s interpretation and attributed this peak to an irreversible phase transition [13]. During this transition, the semi-conducting 2H phase converted into a more metallic 1T phase. This transition seemed to increase the interlayer spacing of MoSe_2 by reducing the vdW forces that exist between the two layers [12]. Al/MoSSe cells showed three distinct plateaus

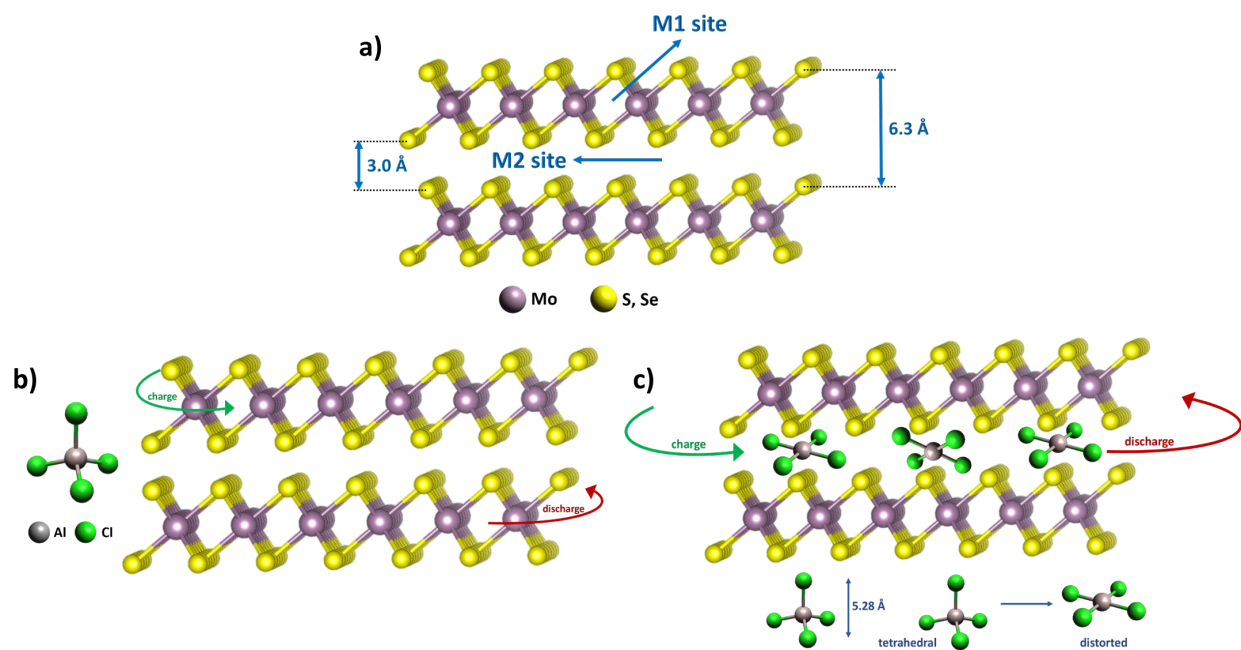


Figure 1: Schematic representation of a) a MoX_2 crystal structure with possible intercalation sites at M1 and M2 b) intercalation at M1 site and c) intercalation at M2 site.

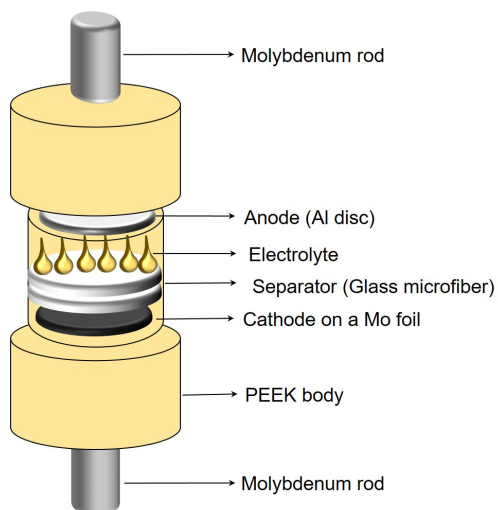


Figure 2: Two-electrode cell assembly using a customised polyether ether ketone (PEEK) body. Molybdenum (Mo) foil was used as the current collector with cathode material coated on top (working electrode) and Mo rods acted as plungers in this Swagelok-type cell. Glass microfibers were used as separators with 99.99% pure Al foil used as anode.

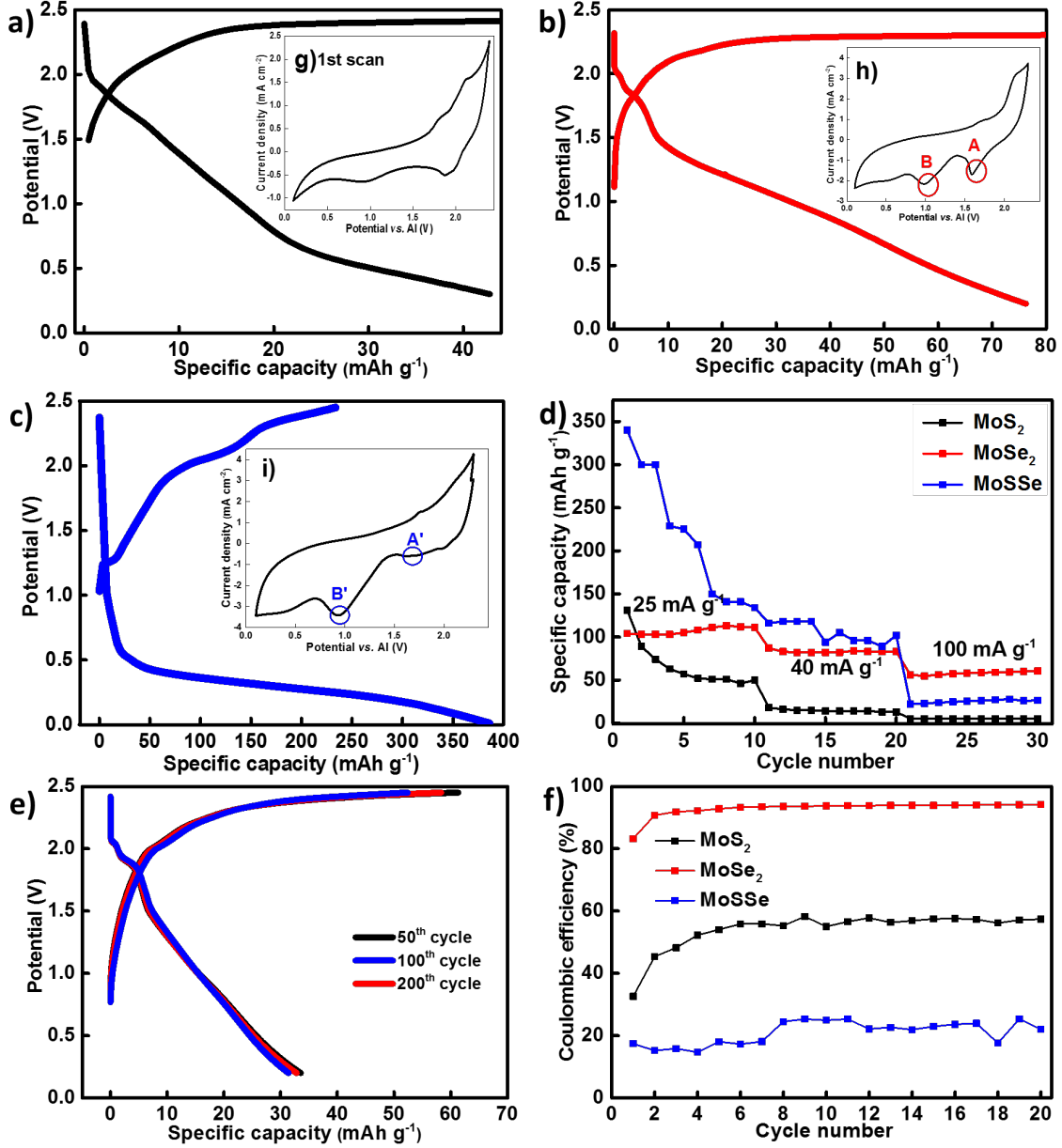


Figure 3: First charge/discharge curve at 40 mA g⁻¹ for a) MoS₂, b) MoSe₂ and c) MoSSe. d) Specific capacities of MoS₂, MoSe₂ and MoSSe at current rates of 25, 40 and 100 mA g⁻¹. e) Coulombic efficiencies of MoS₂, MoSe₂ and MoSSe at a current rate of 100 mA g⁻¹. g) First CV scan of MoS₂, h) MoSe₂ and i) MoSSe at a scan rate of 10 mV s⁻¹ vs. Al/Al³⁺ electrode.

during charging at 1.2 V, 2.0 V and 2.3 V in its first cycle, with a discharge plateau at 0.5 V shown in Figure 3 c). Capacities of all molybdenum dichalcogenides were recorded at different current rates of 25, 40 and 100 mA g⁻¹, and displayed in Figure 3 d). Since MoSe₂ displayed stable specific capacities at all current rates, we recorded further 200 cycles at the highest current rate of 100 mA g⁻¹. A highly reversible electrochemical reaction was observed since the capacity remained at 30-32 mAh g⁻¹ after 200 cycles (Figure 3 e)). The presence of multiple charging plateaus in MoSSe might correspond to various oxidation processes occurring when AlCl₄⁻ interacts individually with S and Se atoms. The first CV scan in Figure 3 i) showed an irreversible reduction potential at 0.9 V, point B', like MoSe₂, implying a similar phase transition. It seems MoSSe undergoes a lattice distortion and the material loses its long range order after converting to its 1T phase. This might be the reason why the cells fail to deliver a stable capacity.

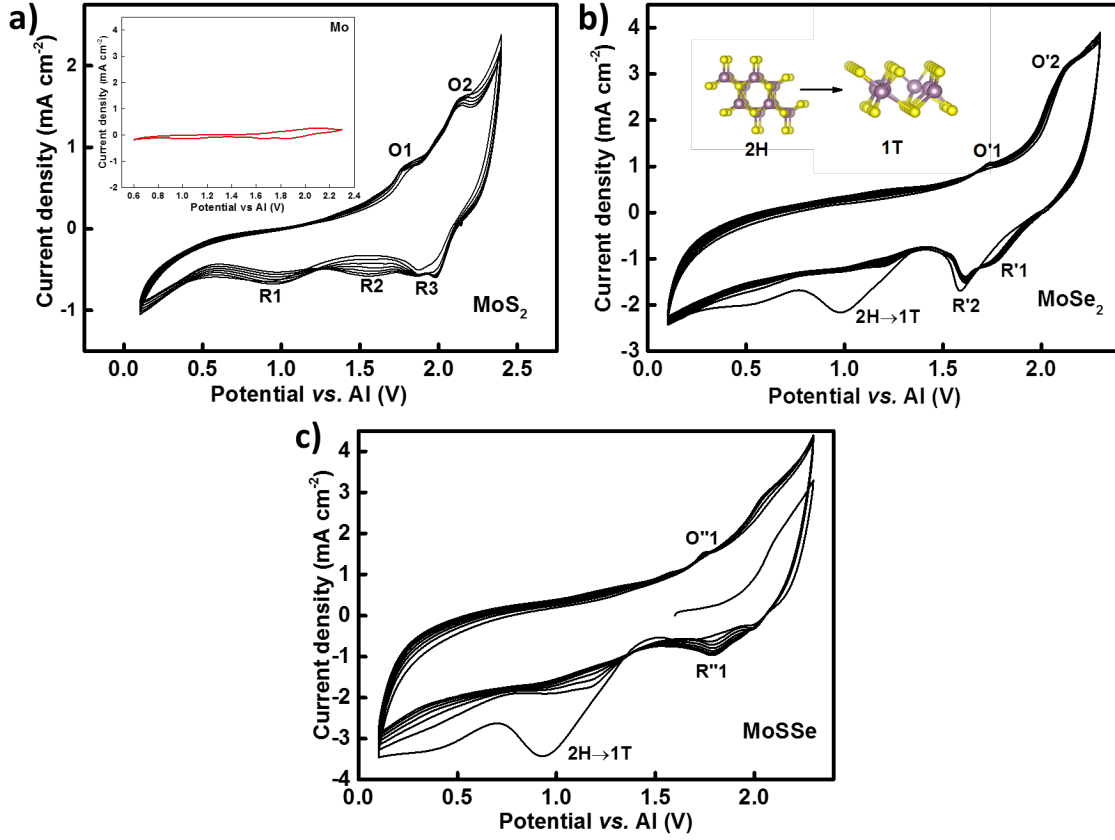


Figure 4: Cyclic voltammograms of a) MoS_2 , b) MoSe_2 and c) MoSSe at a scan rate of 10 mV s^{-1} in a two-electrode aluminium-ion cell against an Al/Al^{3+} reference electrode.

CVs of a blank cell with an uncoated Mo foil (Figure inset 4 a)) showed that the current collector did not contribute to the cell's capacity. Both MoS_2 and MoSe_2 have similar interlayer distance (6.3 \AA) and a gallery height of 3.0 \AA . However, MoSe_2 showed a higher capacity and a more stable cycle life. To account for this behaviour, we compared the cyclic voltammograms of all electrodes at a scan rate of 10 mV s^{-1} in Figure 4. Different charge-storage mechanisms lead to distinct features in the CVs. Ideal capacitors result in a rectangular CV shape. Due to the absence of faradaic processes, the charging/discharging currents are directly proportional to the scan speed. Batteries show oxidation and reduction peaks in their voltammograms [15]. We observed that the CVs of MoSe_2 and MoSSe in Figure 4 b) and 4 c) covered a broader area suggesting an additional capacitor-like charge storage mechanism. This additional non-faradaic process taking place at their surfaces might have resulted in a higher capacity for MoSe_2 and MoSSe . Also, the peak indicating phase transition from $2\text{H} \rightarrow 1\text{T}$ at $\sim 0.9 \text{ V}$ was visible only for MoSe_2 and MoSSe . Charge storage in MoS_2 is primarily based on reversible oxidation and reduction of Mo from Mo^{4+} to Mo^{5+} with oxidation peaks visible at 1.8 V (O1) and 2.1 V (O2), and a corresponding reduction peak at 2.0 V (R3), Figure 4 a). Two more reduction peaks were found at 1.6 V (R2) and 0.9 V (R1). However, their peak intensities decreased with every scan. CV scans of Al/MoSe_2 cells in Figure 4 b) indicated a reversible electrochemical process, which was in agreement with their CDCs. The scans overlapped with each other displaying two oxidation peaks at 1.7 V (O'1) and 2.1 V (O'2) and corresponding reduction peaks at 1.8 V (R'1) and 1.6 V (R'2). In Figure 4 c) an oxidation and a reduction peak at 1.7 V (O''1) and 1.8 V (R''1) was observed for Al/MoSSe respectively. R''1's peak intensity increased after every scan, which might suggest sluggish kinetics in the system; perhaps due to strong interaction between the host material and the intercalating anion. The voltammogram became more capacitor-like after a few scans, indicating the absence of reversible redox processes.

Figure 5 shows the XRD patterns of MoS_2 , MoSe_2 and MoSSe electrodes. Pristine (in black), charged (in green) and discharged (in red) cathodes were compared after 30 cycles. MoS_2 cells displayed a very small shift in their d-spacings. The peak at 14.21° (6.22 \AA) shifted to 14.02° (6.32 \AA), as shown in Figure 5 a). Most of the peaks retained their

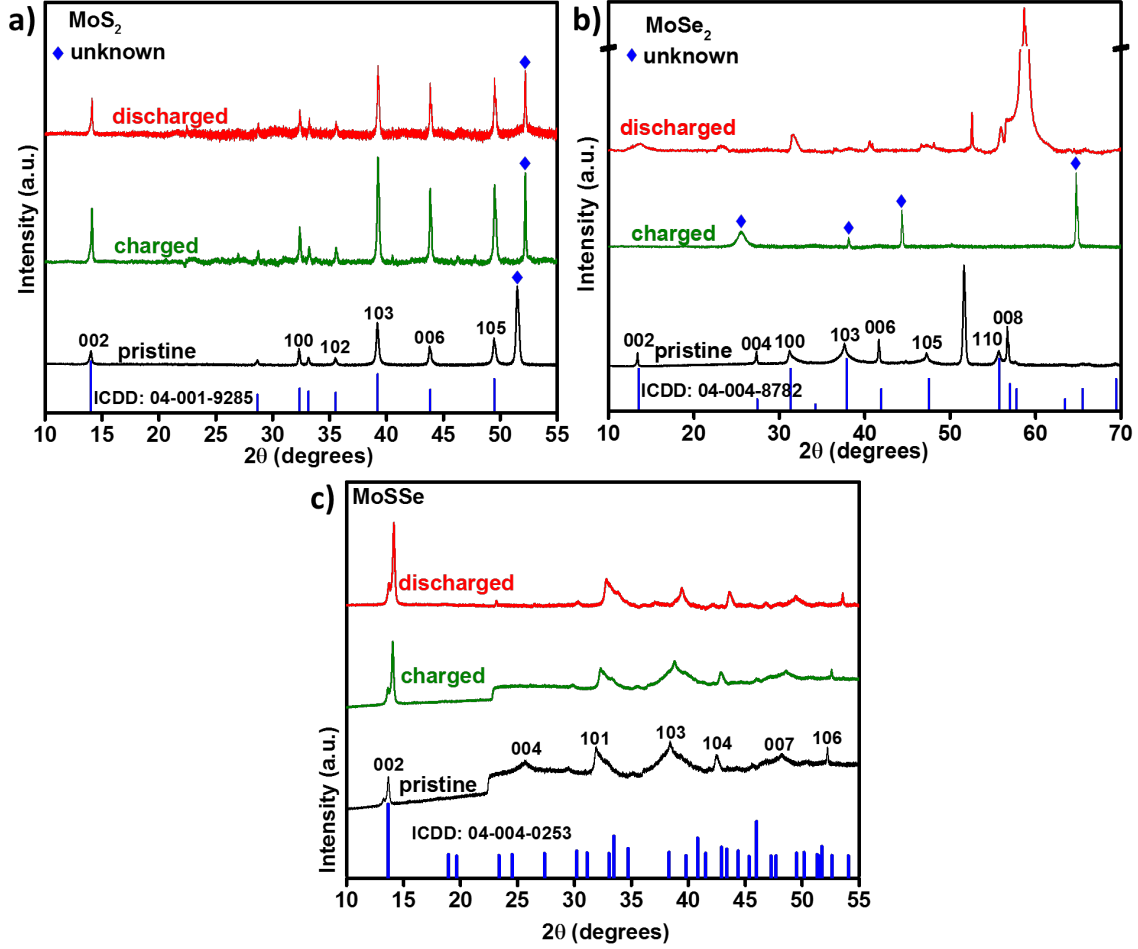


Figure 5: X-ray diffraction patterns of pristine (black), charged (green) and discharged (red) a) MoS_2 , b) MoSe_2 and c) MoSSe electrodes charged to 2.35 V and discharged to 0.2 V vs. Al/Al^{3+} , with International Centre for Diffraction Data (ICDD) references.

positions after charge and discharge showing no significant change in the lattice dimensions. A completely different XRD pattern appeared after charging for Al/MoSe_2 cells, as new peaks appeared at 2θ values, displayed in Figure 5 b). After discharge, the diffraction patterns of the discharged cathodes resembled the pristine cathode patterns. Every time the cells were charged, MoSe_2 seemed to adopt this new crystal lattice. However, the characteristic peaks of MoSe_2 reappeared after discharge. This follows closely the observations made by Rani *et al.* [2], where they proved intercalation of ions into the layers of fluorinated natural graphite during charging. This strongly confirms our hypothesis of a reversible intercalation taking place in MoSe_2 . It was interesting to note that MoSSe did not have a well-defined crystal structure to begin with, Figure 5 c). The patterns after charge and discharge did not look any different from the untested cathode. This confirmed MoSSe layers did not undergo any expansion and the initial specific capacities came from non-faradaic reactions where AlCl_4^- might have been electrostatically absorbed and desorbed onto the surface of the electrode.

To further understand the interactions between AlCl_4^- and MoSe_2 we used XPS, which is a useful method for distinguishing various oxidation states and helps in identifying different polymorphs (2H and 1T) [12]. The detailed narrow spectrum scans in Figure 6 show the binding energies of Mo ($3d_{5/2}$ and $3d_{3/2}$, Figure 6 a) and b)) and Al 2p peaks for charged MoSe_2 (Figure 6 c)) and MoSSe electrodes (Figure 6 d)). In pristine MoSe_2 , two peaks appeared at 229.1 eV and 232.2 eV corresponding to $3d_{5/2}$ and $3d_{3/2}$ (Figure 8 a)). Selenium displayed a doublet at 55.4 eV and 54.6 eV corresponding to Se $3d_{3/2}$ and $3d_{5/2}$ respectively (Figure 8 c)). Peak splitting in an XPS spectrum can indicate a phase change or a change in oxidation state. After charge, the peak for Mo 3d split into three doublets indicating the presence of multiple oxidation states or phases of Mo (Figure 6 a)). Se 3d deconvoluted into four peaks after charge, Figure 8 e), confirming presence of more than one phase after charge. This was similar to observations made by Fan *et*

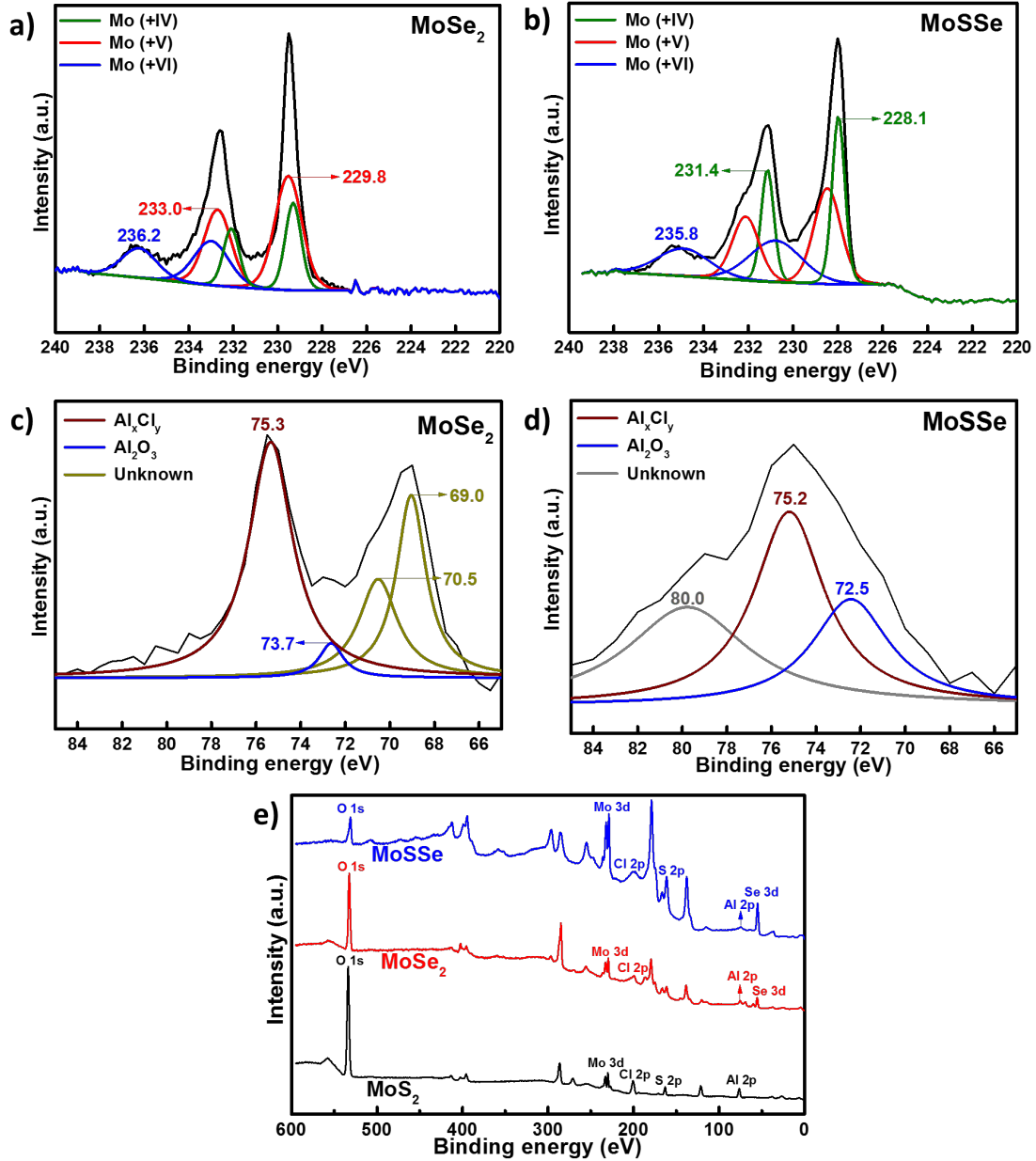


Figure 6: XPS spectra of Mo 3d orbitals in a charged a) MoSe₂ and b) MoSSe cathode and Al 2p orbitals in a charged c) MoSe₂ and d) MoSSe cathode. e) An overview spectrum of all three tested and charged cathodes.

al. Pristine electrodes of MoSSe contained Mo in more than one oxidation state, and provided evidence for the presence of both 2H and 1T polymorphs, Figure 8 b). After charging, the width of peaks at 231.7 eV (Mo 3d_{5/2}) and 228.6 eV (Mo 3d_{3/2}) increased as displayed in Figure 6 b). After comparing Figure 8 d) and f), we noticed that the Se 3d spectrum deconvoluted into four peaks after charging in MoSSe cells. An increase in the peak width was observed for both Mo and Se binding energies. A new peak at ~236 eV in Mo 3d spectra for MoS₂, MoSe₂ and MoSSe electrodes generally indicates a Mo⁶⁺ species present in molybdenum oxide, MoO₃.

The peak shifts detected in Mo 3d spectra for charged MoS₂ and MoSe₂ cathodes were insignificant in MoSSe (cf. Figures 7 a), b), 6 a), and 8 a)). This further confirms the absence of redox reactions and that the capacity was

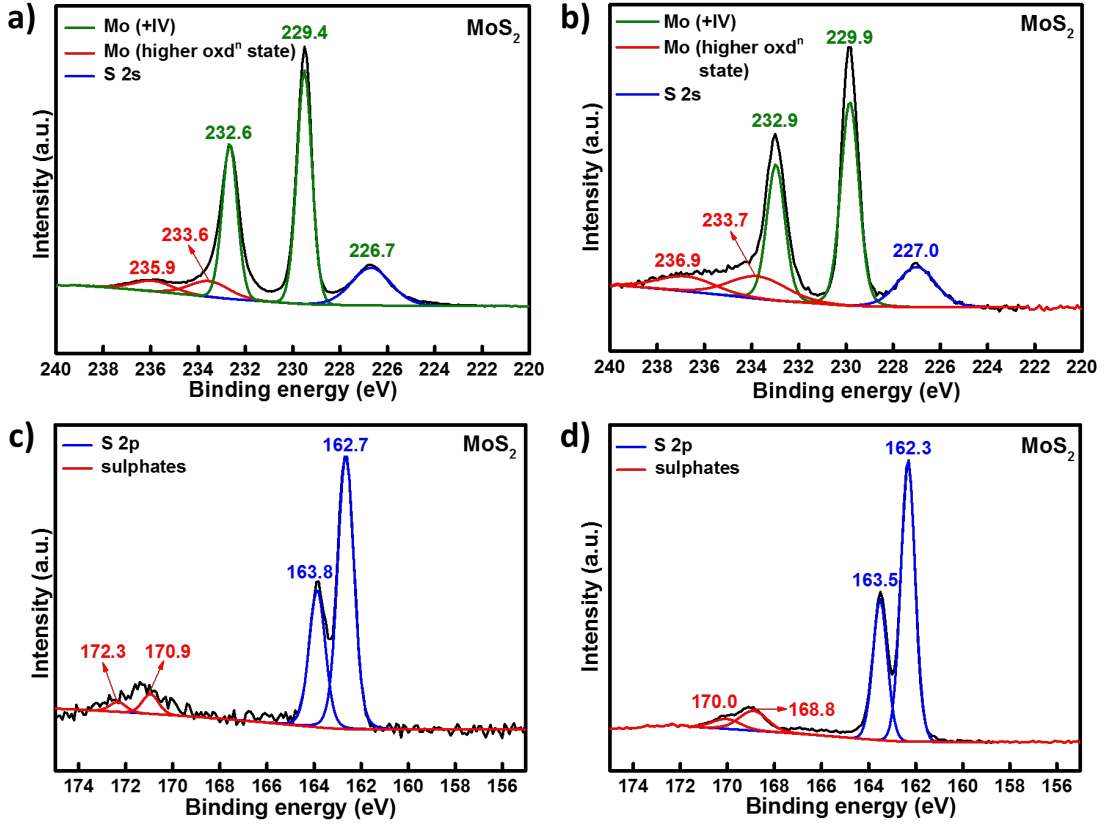


Figure 7: XPS spectra of Mo 3d orbitals in a charged and b) discharged MoS₂ cathode and binding energies of S 2p orbital in a charged and b) discharged MoS₂ cathode.

mainly derived from a surface-based charge storage. As expected, charged electrodes showed higher concentration of aluminium and chlorine than discharged electrodes as seen in Figure 8 g) and h). The XPS spectra support the observation that MoSe₂ underwent a phase transformation that made it a better performing cathode than MoS₂. Further analysis is needed to fully understand the mechanism of MoSSe.

Charged MoSe₂ electrodes displayed binding energies of Al 2p at 77 eV (red) and 76 eV (in blue) corresponding to chlorides (AlxCly) and Al₂O₃ respectively in Figure 6 c). New peaks were observed at much lower binding energies — 69 and 70 eV (green) suggesting the presence of a new complex with an increased electron density around aluminium. An overall spectra of charged MoS₂, MoSe₂ and MoSSe cathodes is shown in Figure 6 e) indicating the presence of Al and Cl (from chloroaluminates) and oxygen (from MoO₃).

In addition, we compared the Raman spectra of pristine and charged cathodes to detect shifts in vibrational modes, Figure 9. E_{2g}^1 and A_g^1 are the most intense vibrational modes for molybdenum dichalcogenides [16, 17, 18]. Peaks corresponding to E_{2g}^1 and A_g^1 modes for MoS₂ (Figure 9 a)) are prominent at 384.6 cm⁻¹ and 410.2 cm⁻¹ respectively. A_g^1 indicates an out-of-plane symmetric displacement of S atoms, whereas E_{2g}^1 suggests an in-layer displacement. Also, separation between the two peaks indicates a multi-layer structure, which was observed for all three materials. No significant peak shift or peak broadening was observed for the charged MoS₂ electrode. For 2H MoSe₂ (Figure 9 b)), A_g^1 is the most intense vibration occurring at a frequency lower than that of E_{2g}^1 . When the number of layers decreases, the A_g^1 mode softens (increase in full-width-at-half-maximum (FWHM)). Spectra generated after intercalation were different from the pristine cathodes because phase conversion from 2H to 1T decreases the molecule's symmetry and more Raman bands get active. The presence of J1 and J2 peaks in addition to E_{2g}^1 and A_g^1 at lower wavelengths suggest the existence of 1T phase especially for MoSe₂ and MoSSe (inset, Figure 9 b) and c)). This agrees with our CV scans where a phase transition was observed for MoSe₂ and MoSSe. Raman results suggest that 'chloroaluminium' or insertion of chloroaluminates changed the symmetry and vibrational modes of MoSe₂'s crystal lattice.

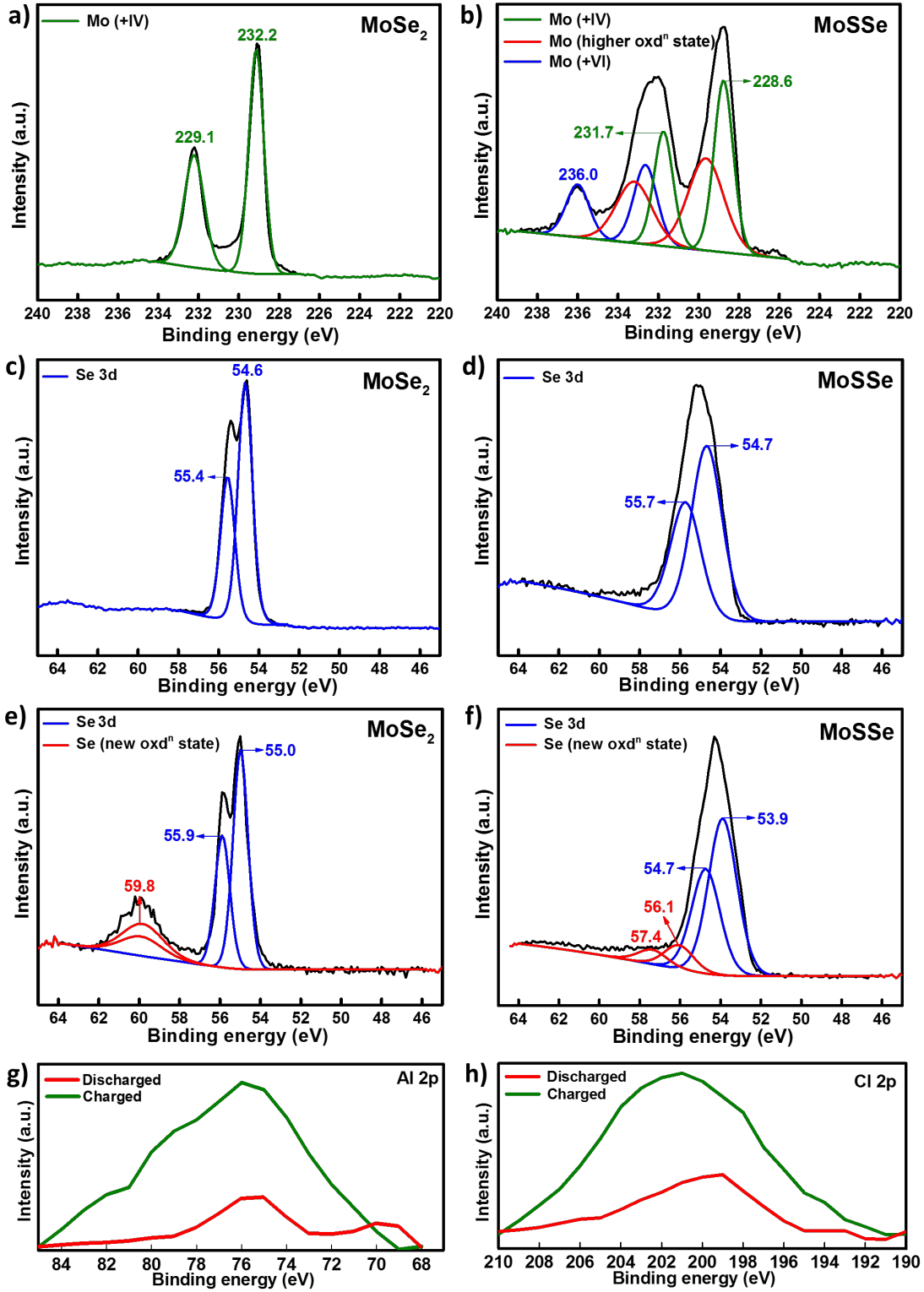


Figure 8: XPS spectra of Mo 3d for pristine a) MoSe₂ and b) MoSSe electrodes. The spectra of MoSe₂ are composed of two peaks at 232.2 eV and 229.1 eV corresponding to Mo⁴⁺. MoSSe spectra consist of three doublet bands, which were assigned to Mo⁴⁺, one with higher oxidation state and another band corresponding to Mo⁶⁺ at 236 eV. c) Pristine and e) charged Se 3d from MoSe₂. MoSe₂ observed peaks corresponding to 3d_{3/2} and 3d_{5/2} at 55.6 eV and 54.6 eV respectively. Binding energies of Se 3d from d) pristine and f) charged MoSSe cathodes.

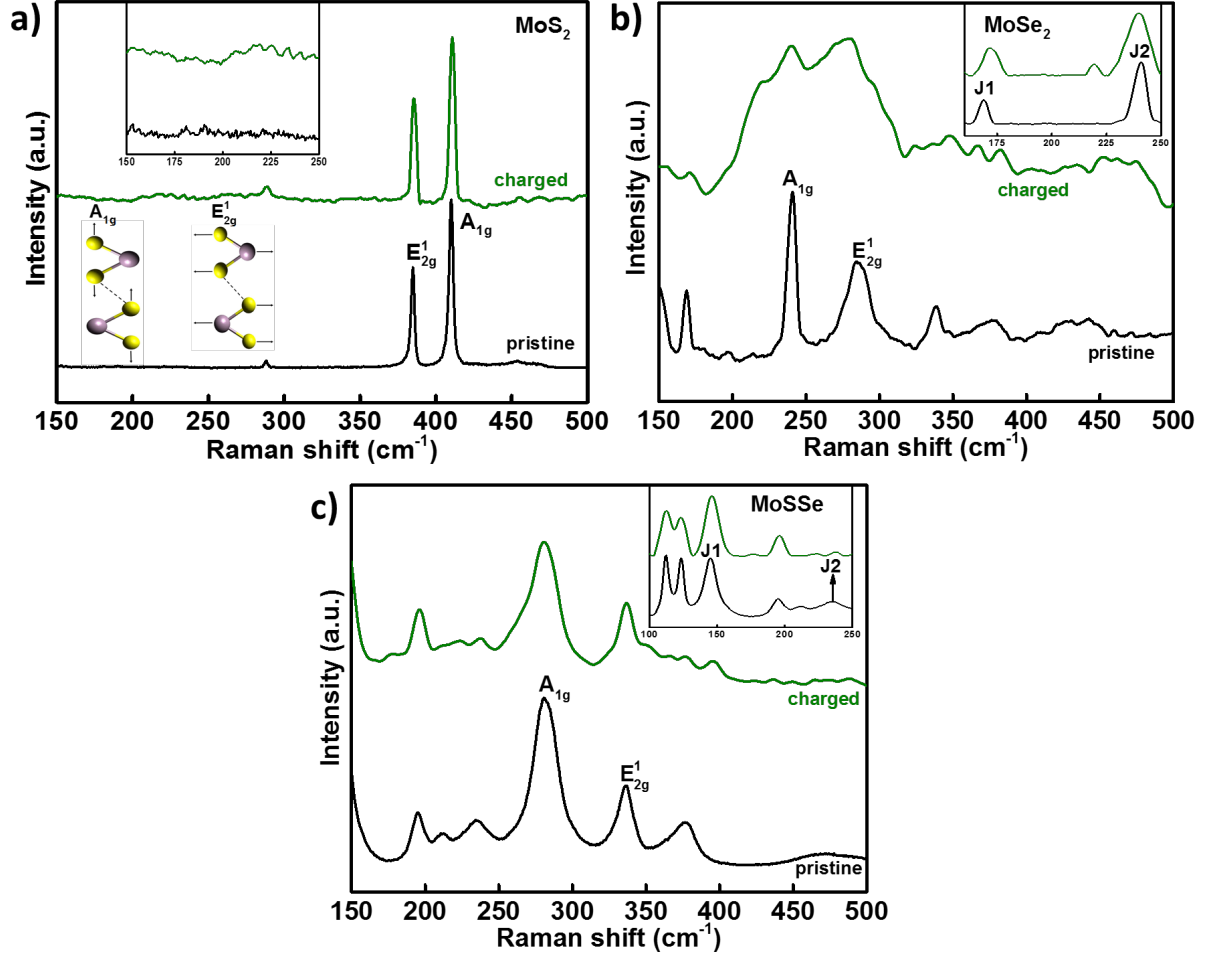


Figure 9: Raman spectra of pristine (black) and charged (green) a) MoS₂, b) MoSe₂ and c) MoSSe electrodes with position of new Raman active J1 and J2 bands marked along with E_{2g}¹ and A_g¹ bands.

3 Conclusions

In this work, we studied systematically the charging/discharging mechanism of aluminium-ion batteries, using different molybdenum dichalcogenide cathodes. It was found that MoSe₂ showed a higher capacity and cyclic stability than MoS₂ and MoSSe. CV and XPS results indicated an irreversible phase transition to a more metallic 1T phase. This transition worked in favour of MoSe₂ and its capacity increased. XRD, XPS and Raman results supported the hypothesis that AlCl₄⁻ intercalated reversibly into MoSe₂. An additional electro-capacitive behaviour was observed in MoSe₂ that added to its overall capacity. The cells delivered a potential of ~ 2.0 V with discharge capacity of 30 mAh g⁻¹ with nearly 95% coulombic efficiency at a current rate of 100 mA g⁻¹.

4 Experimental Section

4.1 Cathode preparation

A slurry was prepared by mixing MoX₂ (85% by wt.), 9% binder (PVDF, MTI Corporation) and 6% Super-P conductive carbon (99+% metals basis, Alfa Aesar) in N-methyl pyrrolidone (NMP) (anhydrous, 99.5%, Sigma-Aldrich). this slurry was ‘doctor-bladed’ onto molybdenum foil (thickness 0.1 mm, MTI Corporation) and dried in a vacuum oven at 120°C for 12 hours to adhere the slurry on the conductive substrate and evaporate the solvent. The specific loading of the active materials was approx. 12 mg cm⁻².

4.2 Electrolyte preparation

Anhydrous AlCl_3 (Sigma-Aldrich) and EMImCl (97%, Sigma-Aldrich) were mixed in a molar ratio of 1.3:1, at room temperature. EMImCl was baked in vacuum for 24 hours at 100°C to remove residual moisture. Small aliquots of AlCl_3 were added to EMImCl after every few minutes until the white fumes settled down. The ionic liquid was stirred for 2–3 hours until a clear brown liquid was obtained. Since the electrolyte was hygroscopic in nature, it was prepared in a N_2 -filled glove box with <0.1 ppm $\text{H}_2\text{O}/\text{O}_2$.

4.3 Cell assembly

Polyether ether ketone (PEEK) cells were used for preliminary electrochemical tests. Molybdenum rods were used as plungers to push in the electrodes as close to each other. Active material coated on molybdenum foil was used as the cathode and placed at bottom of the cell. Since this was a two-electrode setup, aluminium foil was used as both counter and reference electrode. We used Mo foil because nickel and steel showed reactivity towards the ionic liquid electrolyte and reduced its potential window. Glass microfibers (Grade GF/F, Whatman) were used as separators. $80\ \mu\text{l}$ of the electrolyte were used to wet the separator. Aluminium foil (thickness 0.1 mm, 99%, GoodFellow) was used as an anode and placed on top of the separator. The cell was then sealed and wrapped with a paraffin to avoid any further air or moisture contact after it was taken out of the glove-box.

References

- [1] Nicolò Canever, Nicolas Bertrand, and Thomas Nann. Acetamide: A low-cost alternative to alkyl imidazolium chlorides for aluminium-ion batteries. *Chem. Commun.*, September 2018.
- [2] J. Vatsala Rani, V. Kanakaiah, Tulshiram Dadmal, M. Srinivasa Rao, and S. Bhavanarushi. Fluorinated Natural Graphite Cathode for Rechargeable Ionic Liquid Based Aluminum–Ion Battery. *Journal of The Electrochemical Society*, 160(10):A1781–A1784, January 2013.
- [3] Shutao Wang, Kostiantyn V. Kravchyk, Frank Krumeich, and Maksym V. Kovalenko. Kish Graphite Flakes as a Cathode Material for an Aluminum Chloride–Graphite Battery. *ACS Appl Mater Interfaces*, 9(34):28478–28485, August 2017.
- [4] Meng-Chang Lin, Ming Gong, Bingan Lu, Yingpeng Wu, Di-Yan Wang, Mingyun Guan, Michael Angell, Changxin Chen, Jiang Yang, Bing-Joe Hwang, and Hongjie Dai. An ultrafast rechargeable aluminium-ion battery. *Nature*, 520(7547):324–328, April 2015.
- [5] Jia Qiao, Haitao Zhou, Zhongsheng Liu, Hejing Wen, and Jianhong Yang. Defect-free soft carbon as cathode material for Al-ion batteries. *Ionics*, February 2019.
- [6] Yanliang Liang, Rujun Feng, Siqi Yang, Hua Ma, Jing Liang, and Jun Chen. Rechargeable Mg Batteries with Graphene-like MoS_2 Cathode and Ultrasmall Mg Nanoparticle Anode. *Adv. Mater.*, 23(5):640–643, 2011.
- [7] Junda Huang, Zengxi Wei, Jiaqin Liao, Wei Ni, Caiyun Wang, and Jianmin Ma. Molybdenum and tungsten chalcogenides for lithium/sodium-ion batteries: Beyond MoS_2 . *Journal of Energy Chemistry*, 33:100–124, June 2019.
- [8] Xiao-Lin Li and Ya-Dong Li. MoS_2 Nanostructures: Synthesis and Electrochemical Mg^{2+} Intercalation. *J. Phys. Chem. B*, 108(37):13893–13900, September 2004.
- [9] Changbao Zhu, Xiaoke Mu, Peter A. van Aken, Joachim Maier, and Yan Yu. Fast Li Storage in MoS_2 -Graphene-Carbon Nanotube Nanocomposites: Advantageous Functional Integration of 0D, 1D, and 2D Nanostructures. *Adv. Energy Mater.*, 5(4):n/a–n/a, February 2015.
- [10] Linxiao Geng, Guocheng Lv, Xuebing Xing, and Juchen Guo. Reversible Electrochemical Intercalation of Aluminum in Mo_6S_8 . *Chem. Mater.*, 27(14):4926–4929, July 2015.
- [11] Zhanyu Li, Bangbang Niu, Jian Liu, Jianling Li, and Feiyu Kang. Rechargeable Aluminum-Ion Battery Based on MoS_2 Microsphere Cathode. *ACS Appl. Mater. Interfaces*, 10(11):9451–9459, March 2018.
- [12] Xin Fan, Rohit Ranganathan Gaddam, Nanjundan Ashok Kumar, and Xiu Song Zhao. A Hybrid $\text{Mg}^{2+}/\text{Li}^+$ Battery Based on Interlayer-Expanded MoS_2 /Graphene Cathode. *Adv. Energy Mater.*, 7(19), October 2017.
- [13] Yifei Li, Yanliang Liang, Francisco C. Robles Hernandez, Hyun Deog Yoo, Qinyou An, and Yan Yao. Enhancing sodium-ion battery performance with interlayer-expanded MoS_2 -PEO nanocomposites. *Nano Energy*, 15:453–461, July 2015.

- [14] Katsunori Takahashi, Ying Wang, and Guozhong Cao. Ni-V₂O₅·nH₂O Core-Shell Nanocable Arrays for Enhanced Electrochemical Intercalation. *J. Phys. Chem. B*, 109(1):48–51, January 2005.
- [15] Handong Jiao, Junxiang Wang, Jiguo Tu, Haiping Lei, and Shuqiang Jiao. Aluminum-Ion Asymmetric Supercapacitor Incorporating Carbon Nanotubes and an Ionic Liquid Electrolyte: Al/AlCl₃-[EMIm]Cl/CNTs. *Energy Technol.*, 4(9):1112–1118, September 2016.
- [16] Linfei Yang, Lidong Dai, Heping Li, Haiying Hu, Kaixiang Liu, Chang Pu, Meiling Hong, and Pengfei Liu. Pressure-induced metallization in MoSe₂ under different pressure conditions. *RSC Adv.*, 9(10):5794–5803, 2019.
- [17] Rao C. N. R and Waghmare Umesh Vasudeo. *2d Inorganic Materials Beyond Graphene*. World Scientific, August 2017.
- [18] Chithra H. Sharma, Ananthu P. Surendran, Abin Varghese, and Madhu Thalakulam. Stable and scalable 1T MoS₂ with low temperature-coefficient of resistance. *Sci Rep*, 8, August 2018.

Supporting Information

Molybdenum dichalcogenide cathodes for aluminium-ion batteries

Shalini Divya, James H. Johnston, Thomas Nann*

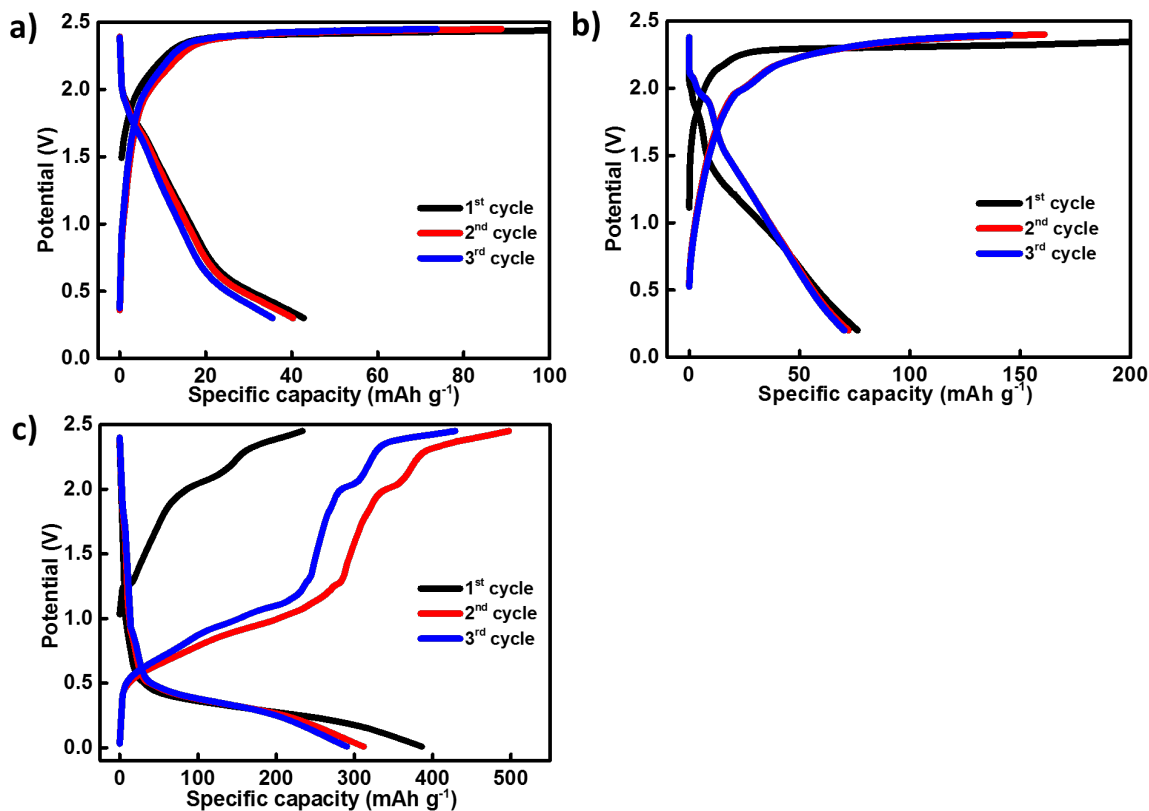


Figure 10: Galvanostatic charge/discharge profile of the first three cycles of a) MoS₂, b) MoSe₂ and c) MoSSe at a current rate of 40 mA g⁻¹ in a two-electrode setup.

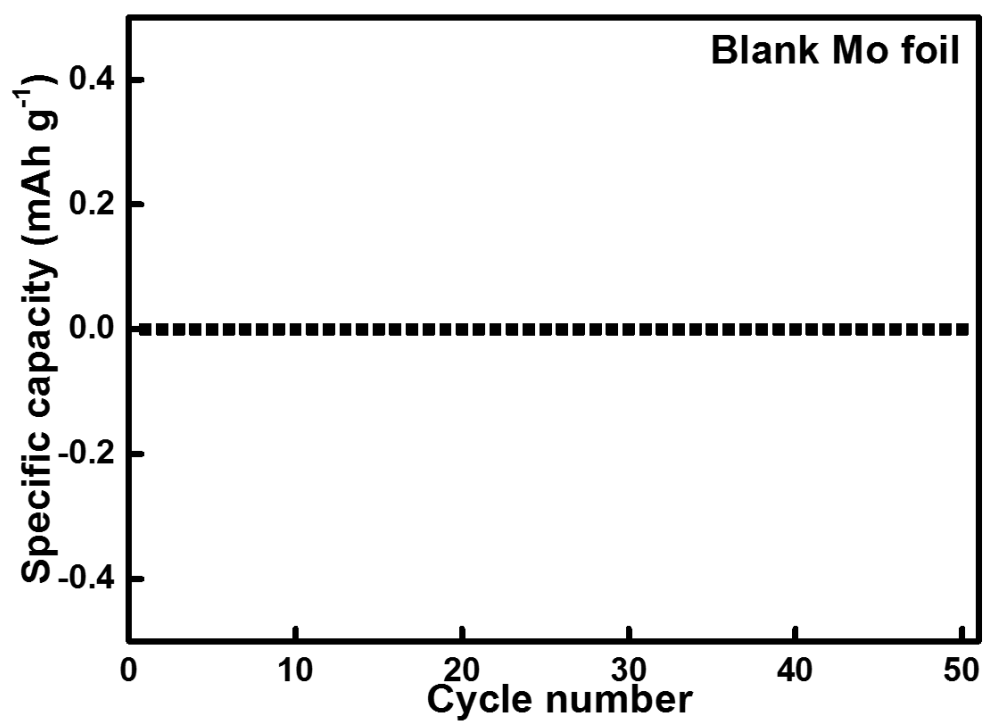


Figure 11: Rate performance of an aluminium-ion cell using blank molybdenum foil as a cathode.